Finite width effect of thin-films buckling on compliant substrate: Experimental and theoretical studies

Hanqing Jiang [a,*], Dahl-Young Khang [b,1], Huiyang Fei [a], Hoonsik Kim [b], Yonggang Huang [c,d], Jianliang Xiao [d], John A. Rogers [b,**]

[a] *Department of Mechanical and Aerospace Engineering, Arizona State University, Tempe, AZ 85287, USA*
[b] *Department of Materials Science and Engineering, Beckman Institute for Advanced Science and Technology, Frederick Seitz Materials Research Laboratory, University of Illinois at Urbana-Champaign, Urbana, IL 61801, USA*
[c] *Department of Civil and Environmental Engineering, Northwestern University, Evanston, IL 60208, USA*
[d] *Department of Mechanical Engineering, Northwestern University, Evanston, IL 60208, USA*

A B S T R A C T

Buckling of stiff thin films on compliant substrates has many important applications ranging from stretchable electronics to precision metrology and sensors. Mechanics plays an indispensable role in the fundamental understanding of such systems. Some existing mechanics models assume plane-strain deformation, which do not agree with experimental observations for narrow thin films. Systematic experimental and analytical studies are presented in this paper for finite-width stiff thin films buckling on compliant substrates. Both experiments and analytical solution show that the buckling amplitude and wavelength increase with the film width. The analytical solution agrees very well with experiments and therefore provides valuable guide to the precise design and control of the buckling profile in many applications. The effect of film spacing is studied via the analytical solutions for two thin films and for periodic thin films.

© 2008 Elsevier Ltd. All rights reserved.

1. Introduction

Ordered buckling structures in thin metal films on elastomeric substrates, first reported by Bowden et al. (1998), have broad applications ranging from stretchable electronic interconnects (Lacour et al., 2003, 2004, 2005, 2006; Wagner et al., 2004) and stretchable electronic devices (Choi and Rogers, 2003; Khang et al., 2006; Choi et al., 2007; Jiang et al., 2007a, b), microelectromechanical systems (MEMS) and nanoelectromechanical systems (NEMS) (Fu et al., 2006), and tunable diffraction and phase gratings (Harrison et al., 2004; Efimenko et al., 2005), to force spectroscopy in cells (Harris et al., 1980), biocompatible topographic matrices for cell alignment (Jiang et al., 2002; Teixeira et al., 2003), modern metrology methods (Stafford et al., 2004, 2005, 2006; Wilder et al., 2006), and methods for micro/nano-fabrication (Bowden et al., 1998, 1999; Huck et al., 2000; Sharp and Jones, 2002; Yoo et al., 2002; Schmid et al., 2003). Thin buckled films on elastomeric supports exist in several different geometries. The first is to deposit metals onto an elastomer (Bowden et al., 1998), which leads to sinusoidal wave patterns and networks of micro/nanocracks in the metal. The second uses the transfer of solid films or ribbons created on a separate growth substrate onto the elastomer (Khang et al., 2006; Choi et al.,

2007; Jiang et al., 2007a), in a manner that yields well-controlled sinusoidal geometries. Fig. 1 shows a schematic illustration of the procedures for forming buckled ribbons of single crystalline Si on a PDMS substrate. Wide-ranging classes of materials are possible, including even brittle single crystalline semiconductors such as silicon and gallium arsenide (Khang et al., 2006), without cracking. These two classes of configurations, both involve strong bonding of the
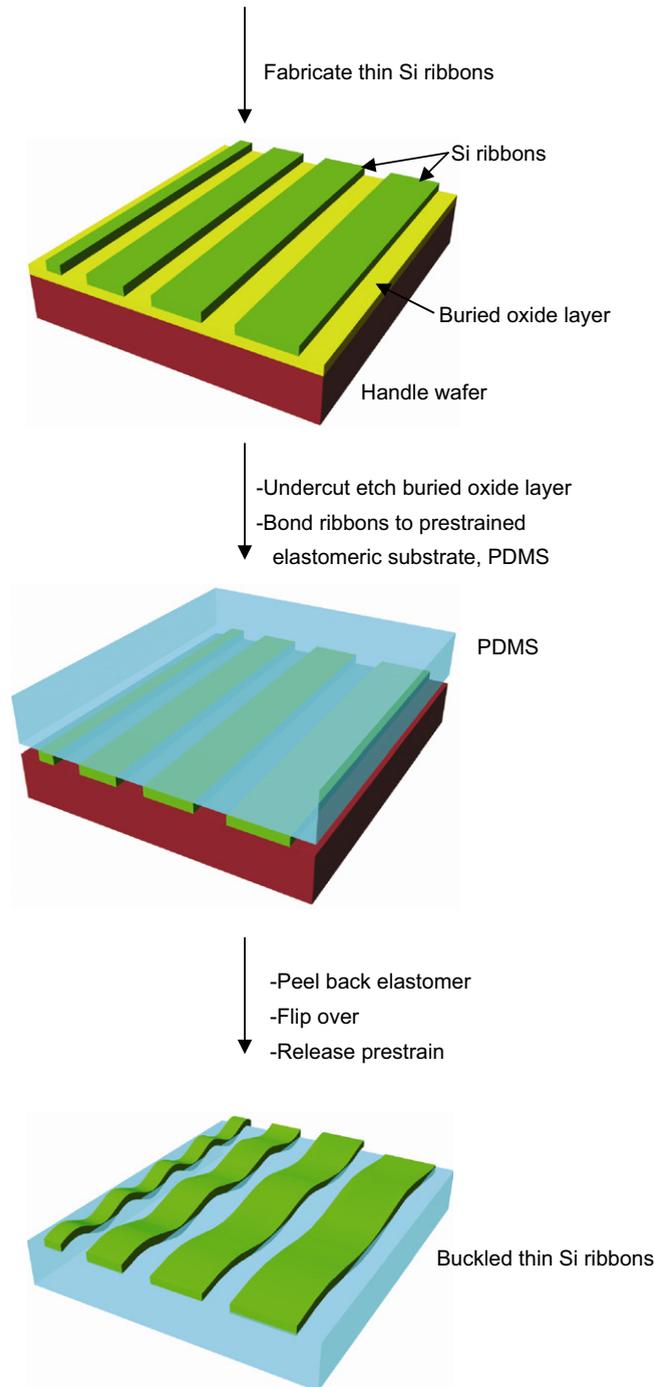
Fig. 1. Schematic illustration of experimental procedures for the buckling of single crystalline Si ribbons on elastomeric substrates, poly(dimethylsilox-ane) (PDMS). After patterning the top Si layer of silicon-on-insulator (SOI) wafer into the ribbon shape (top panel), the oxide layer undercut etched to release Si ribbons. Placing surface treated (uv/ozone), prestretched (heating to 70 °C) flat slab of PDMS on the SOI wafer results in a strong chemical bonding between Si and PDMS (middle). Peeling off the PDMS from the wafer transfers the Si ribbons onto the PDMS. The Si ribbons become buckled into a sinusoidal, wavy shape when the Si/PDMS is cooled down to room temperature (bottom). Note here that the ribbon width effect on the buckling profile is also shown; the wider the ribbon, the larger the buckling wavelength.

films to the substrates at all points along their interface. Spatially modulating this adhesion through lithographically patterned surface chemistry enables a third class of buckled system (Sun et al., 2006; Jiang et al., 2007b). The films buckle in controlled geometries that involve intimate mechanical contact at the adhesion sites and physical separations in the other regions. In all three cases, thermal or mechanical methods are used to stretch the elastomeric substrate, such as poly(dimethylsiloxane) (PDMS), prior to deposition or transfer such that relaxing the pre-strain in the substrate yields the compressive strain in thin films, which leads to buckling of thin films in order to release the compressive strain.

Mechanics models have been developed to understand these systems (e.g., Huang and Suo, 2002a, b; Huang et al., 2002, 2004, 2005; Huang, 2005; Huang and Im, 2006). One of the primary goals of these theoretical studies is to identify the relation between buckling profile (i.e., wavelength and amplitude) and other material parameters (e.g., materials moduli, dimensional parameters) because the buckling profile is critical in many applications. For example, in modern metrology methods, the measured buckling wavelength is used to determine the modulus of thin film or substrate (Stafford et al., 2004, 2005, 2006; Wilder et al., 2006). The wavelength and amplitude are also very important for flexible and stretchable electronics since they are closely related to the achievable maximum stretchability, which is the most critical quantity in stretchable electronics. The existing mechanics models (e.g., Huang et al., 2005) give analytically the buckling wavelength λ_0:

$$\lambda_0 = 2\pi h \left(\frac{\bar{E}_f}{3\bar{E}_s}\right)^{\frac{1}{3}}, \tag{1}$$

and amplitude A_0 as

$$A_0 = h\sqrt{\frac{\varepsilon_{pre}}{\varepsilon_c} - 1}, \tag{2}$$

where h is the thin-film thickness,

$$\varepsilon_c = \frac{1}{4}\left(\frac{3\bar{E}_s}{\bar{E}_f}\right)^{\frac{2}{3}} \tag{3}$$

is the critical strain for buckling (i.e., the thin films buckle once the pre-strain $\varepsilon_{pre} > 0$ reaches ε_c), $\bar{E}_s = E_s/(1-v_s^2)$ and $\bar{E}_f = E_f/(1-v_f^2)$, E_s, E_f, v_s, and v_f are the plane-strain moduli, the Young's moduli and the Poisson's ratios of the substrate and thin film, respectively. Eqs. (1) and (2) agreed reasonably well with experiments (e.g., Khang et al., 2006), and have been widely used as in modern metrology methods (Stafford et al., 2004, 2005, 2006; Wilder et al., 2006).

Eqs. (1) and (2), however, involve one critical assumption that the thin-film width (the dimension perpendicular to the pre-strain direction) is much larger than the wavelength such that the deformation is plane strain. However, this assumption does not hold in many applications. For instance, the thin film in stretchable metal interconnects (Lacour et al., 2005) is a one-dimensional-like stripe, for which the plane-strain assumption does not hold. Another experiment that showed the important effect of film width is the buckling of ultrananocrystalline diamond (UNCD) thin films on PDMS substrate (Kim et al., 2008). Fig. 2 shows a buckled system of a 440 nm thick and 10-μm-wide UNCD film on a 4-mm-thick PDMS substrate. The buckling wavelength was 85 μm in the experiment, while Eq. (1) gives the buckling wavelength 118 μm for the Young's modulus 800 GPa and the Poisson's ratio 0.07 of UNCD (Espinosa et al., 2003). This large discrepancy between the theory and experiment is due to the neglect of the finite film width effect in the existing mechanics models. Our own experiments to be discussed in Section 2 also show the strong effect of film width.

A nonlinear buckling model is presented in this paper for the buckling of thin films with finite width on compliant substrates. Our recent experiments that reveal the width effects on the buckling wavelength are described in Section 2.
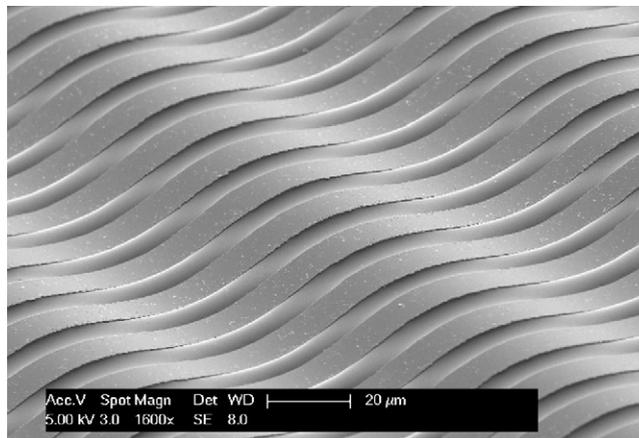
Fig. 2. Angled-view scanning electron microscopy (SEM) images of wavy diamond ribbons on PDMS substrate.

The method of energy minimization is described in Section 3, along with the energies in the thin film and substrate. Energy minimization gives the buckling wavelength and amplitude that are compared with experiments in Section 4. The effect of film spacing is studied in Section 5, and the analytical results are compared with experiments. The effect of periodic ribbons on buckling profile is studied in Section 6.

2. Experiments: strong width effect

Fig. 1 illustrates the fabrication procedures. Single-crystalline Si (1 0 0) ribbons are derived from silicon-on-insulator (SOI) wafers (SOItec Inc.), with top Si thicknesses of 100 nm. The first step involves patterning a layer of photoresist (AZ5214) in the geometry of ribbons on top of an SOI wafer using conventional photolithographic methods (Karl Suss MJB-3 contact mask aligner). The ribbon width systematically varies from 2 to 200 μm, while their length is fixed at 15 mm for all cases. In order to remove any possible mechanical coupling effect between neighboring ribbons, the spacing between ribbons is fixed at five times larger than their widths (for example, 5-μm-wide ribbons spaced apart 25, and 100-μm-wide ribbons with spacing of 500 μm). For experiments that examine the effects of spacing, the ribbon widths are fixed at 8 or 11 μm, while the spacing varies up to about 30 μm. Etching the exposed top Si layer by SF_6 reactive ion etching (PlasmaTherm) defines the ribbons (Fig. 1, top frame). Undercut etching of buried oxide layer with HF releases the Si ribbons and leaves them resting on the underlying Si substrate.

The PDMS (Sylgard 184, Dow) substrates are formed by casting and thermally curing (70 °C for >4 h) at 10:1 (by weight) mixture of base resin to curing agent against a surface functionalized silicon wafer. Flat slabs of PDMS (3–5 mm thick) formed in this manner serve as the substrates. The process for integrating Si ribbons on the PDMS substrates begins with an exposure of the PDMS to ultraviolet-induced ozone for 1–2 min to create surface –OH groups. The PDMS is then heated to 70 °C inside an oven, which resulted in a moderate pre-stretching due to thermal expansion. Placing a processed SOI wafer against this pre-stretched PDMS, and then removing the wafer transferred the Si ribbons to the PDMS through the action of strong, covalent –O–Si–O– bonds that form at the interface.

The transfer and bonding processes are done inside the oven, which is maintained at 70 °C (middle frame in Fig. 1), to minimize any temperature fluctuation. In order to avoid bonding between the PDMS and the silicon wafer of the SOI
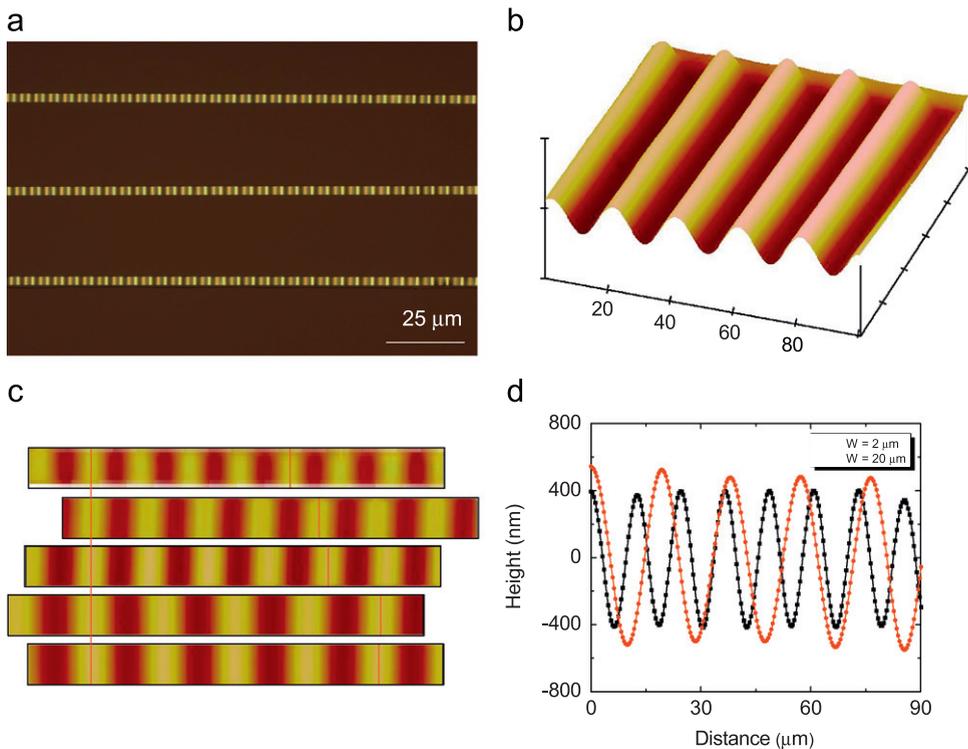
Fig. 3. Some representative experimental results on the width-dependent buckling profile. (a) Optical microscopy image of buckled 5-μm-wide Si ribbons (spaced 25 μm apart) on PDMS (scale bar = 25 μm). (b) Three-dimensional atomic force microscope (AFM) perspective view of buckled 100-μm-wide Si ribbons. (c) Stacked plane-view AFM images of buckled Si ribbons, having different widths of 2, 5, 20, 50, and 100 μm (from top to bottom). A wave peak in each image is aligned at the left and marked with a long, red line, and their fourth peaks are marked with short red lines indicating the variation of the wavelength with respect to the ribbon width. It can be clearly seen that the wavelength increases and then seems to saturate at/above certain value, as the Si ribbon width increases. (d) AFM line-cut profiles along the buckled wavy Si ribbons for 2 μm (black) and 20 μm (red) wide ribbons. For comparison purpose, those profiles are shifted to have peaks at the same origin; again, the wavelength and amplitude increase as the ribbon width increases.

substrate (i.e., the handle wafer), the contact between the PDMS and the processed SOI is limited to ∼1 min. We found that this contact time (∼1 min) ensured transfer-bonding of Si ribbons from processed SOI wafer onto PDMS, while preventing unwanted bonding between PDMS and SOI substrate. After peeling back the PDMS from the SOI wafer with the Si ribbons on its surface, the bonding is allowed to run to completion (>10 min at 70 °C) before releasing or applying strains. As the sample is cooled down to room temperature, the Si ribbons become buckled by the compressive stress caused by shrinkage of PDMS substrate (Fig. 1, bottom frame). An optical microscope is used to determine the wavelength by measuring the distance between two fixed points in the image and dividing it by the number of waves in between. Atomic force microscopy (DI 3100, Veeco) is used to determine the wave amplitude, and also serves to verify the measured wavelength by optical microscopy.

Fig. 3 shows some experimental results of the ribbon width effect on the buckling profile. An optical microscope image of buckled, 5-μm-wide Si ribbons (25 μm spacing) is shown in Fig. 3(a),three-dimensional AFM perspective view of a buckled 100-μm-wide ribbon in Fig. 3(b). In Fig. 3(c), plane-view AFM images of Si ribbons with different widths (2, 5, 20, 50, and 100 μm, from top to bottom) are stacked together. The peaks of waves in each ribbon are aligned at the left side and marked with long, vertical red lines, and fourth wave peaks are marked with short red lines on each ribbon. From this series of images, the variation of wavelength can clearly be seen; the wavelength increases with the ribbon width, and then seems to saturate at a finite value. For the quantitative comparison of wave profile for each ribbon width, the linecut profiles from the AFM measurements are replotted in Fig. 3(d) for the 2- and 20-μm-wide ribbons. The data are shifted to make the peaks at the same location, thereby making it easy to observe that the buckling amplitude and wavelength increase with the ribbon width, i.e., strong ribbon width effect.

3. Energy for the thin film/substrate system

A single thin film of width W on a compliant substrate is studied in this section, while the interactions among thin films, i.e., the effect of thin film spacing, will be studied in Sections 5 and 6. The total energy consists of three parts, namely the thin film bending energy U_b due to buckling, thin film membrane energy U_m, and substrate energy U_s.

3.1. Thin film

The thin film is modeled as an elastic beam because the film thickness (∼100 nm) is much smaller than any other characteristic lengths in the film such as the buckling wavelength (∼15 μm), film width (2–200 μm) and length (∼15 mm). As will be shown later, the thin film membrane strain remains to be negligibly small so that the von Karman beam theory (Timoshenko and Gere, 1961) is used to account for the finite rotation effect in buckling analysis. The membrane strain in the beam is

$$\varepsilon_{11} = u_{,1} + \frac{1}{2}(w_{,1})^2, \tag{4}$$

where u is the displacement along the direction of the pre-strain, and w is the out-of-plane displacement. The linear elastic constitutive model gives the axial force

$$N_{11} = WhE_f\varepsilon_{11}. \tag{5}$$

The shear traction T_1 and normal traction T_3 at the film/substrate interface can be obtained from the equilibrium of forces as (Timoshenko and Gere, 1961)

$$T_1 = \frac{\partial N_{11}}{\partial x_1}, \tag{6}$$

and

$$T_3 = D\nabla^2 w - N_{11}w_{,11} - N_{11,1}w_{,1}, \tag{7}$$

where $D = Wh^3E_f/12$ is bending rigidity for film.

Huang et al. (2005) showed that the shear stress at the interface between the stiff thin film and compliant substrate has a negligible effect on the system buckling, and therefore can be neglected, $T_1 \approx 0$. Eq. (6) then gives constant axial force N_{11}, and constant membrane strain ε_{11}.

The buckling profile of the thin film can be expressed as

$$w = A\cos(kx_1), \tag{8}$$

where the amplitude A and wave number k are to be determined, and $\lambda = 2\pi/k$ is the buckling wavelength. The constant membrane strain then gives the axial displacement $u = kA^2\sin(2kx_1)/8$, where the condition $\int_0^{2\pi/k} u_{,1}\,dx = 0$ has been imposed to be consistent with the overall substrate deformation (Chen and Hutchinson, 2004). The membrane strain then becomes $\varepsilon_{11} = 1/4A^2k^2 - \varepsilon_{pre}$, where $-\varepsilon_{pre}$ is the compressive strain due to the relaxation of pre-strain ε_{pre} in the substrate.

For the buckling profile in Eq. (8), the bending energy per unit wavelength of the thin film becomes

$$U_{\mathrm{b}} = \frac{k}{2\pi} \int_0^{\frac{2\pi}{k}} \frac{1}{2} D \left(\frac{\partial^2 w}{\partial x_1^2} \right)^2 \mathrm{d}x_1 = \frac{h^3 E_f W}{48} k^4 A^2. \tag{9}$$

The membrane energy per unit wavelength of the thin film is given by

$$U_{\mathrm{m}} = \frac{1}{2} N_{11} \varepsilon_{11} = \frac{1}{2} W h E_{\mathrm{f}} \left(\frac{1}{4} A^2 k^2 - \varepsilon_{\mathrm{pre}} \right)^2. \tag{10}$$

The normal traction T_3 at the film/substrate interface becomes

$$T_3 = -\beta W \cos(kx_1), \tag{11}$$

where

$$\beta = -\frac{h^3 E_{\mathrm{f}}}{12} A k^4 - h E_{\mathrm{f}} \left(\frac{1}{4} A^2 k^2 - \varepsilon_{\mathrm{pre}} \right) A k^2. \tag{12}$$

3.2. Substrate

The PDMS substrate is modeled as a semi-infinite elastic solid because its thickness (3–5 mm) is 4 orders of magnitude larger than the film thickness (100 nm). The top surface of the PDMS substrate is traction free except within the strip of width W underneath the thin film. The normal traction, $-T_3$ [which is opposite to the stress traction T_3 given in Eq. (11)], is assumed to be uniform over the width W (but non-uniform along the film direction x_1), which gives the following non-vanishing normal stress traction on the top surface of PDMS substrate

$$P = -\frac{T_3}{W} = \beta \cos(kx_1) \tag{13}$$

over the width W, as illustrated in Fig. 4. As shown in the Appendix, this assumption of uniform normal traction over the film width is justified.

Based on the divergence theorem, the strain energy per unit wavelength in the PDMS substrate is

$$U_{\mathrm{s}} = \frac{k}{2\pi} \cdot \frac{1}{2} \int_V \sigma_{ij} \varepsilon_{ij} \, \mathrm{d}V = \frac{k}{4\pi} \int_{-W/2}^{W/2} \int_0^{2\pi/k} P w_{\mathrm{s}} \, \mathrm{d}x_1 \, \mathrm{d}x_2, \tag{14}$$

where w_{s} is the normal displacement on the top surface ($x_3 = 0$) of PDMS substrate, which is obtained analytically in the following from the Boussinesq's solution (Kachanov et al., 2003).

For a unit normal point force at ($t_1, t_2, 0$) on the surface of an incompressible semi-infinite solid, the Boussinesq's solution gives the normal displacement at ($x_1, x_2, 0$) on the surface as $(1/\pi \bar{E}_s) 1/\sqrt{(x_1 - t_1)^2 + (x_2 - t_2)^2}$. For the distributed load in Eq. (13), the normal displacement on the surface is the integration over the entire thin film area,

$$\begin{aligned} w_{\mathrm{s}}(x_1, x_2, 0) &= \int_{-W/2}^{W/2} \int_{-\infty}^{\infty} \frac{\beta \cos(kt_1)}{\pi \bar{E}_s} \frac{1}{\sqrt{(x_1 - t_1)^2 + (x_2 - t_2)^2}} \, \mathrm{d}t_1 \, \mathrm{d}t_2 \\ &= 2 \int_{-W/2}^{W/2} \frac{\beta \cos(kx_1)}{\pi \bar{E}_s} Y_0(k|t_2 - x_2|) \, \mathrm{d}t_2, \end{aligned} \tag{15}$$

where Y_n ($n = 0, 1, 2, \ldots$) is the modified Bessel function of the second kind (Abramowitz and Stegun, 1972). Because the film/substrate interface is replaced by the normal traction in Eq. (13), the above displacement on the surface of the PDMS substrate is continuous with the displacement in Eq. (8) for the thin film only on the average sense, which is to be further discussed in Section 3.3.
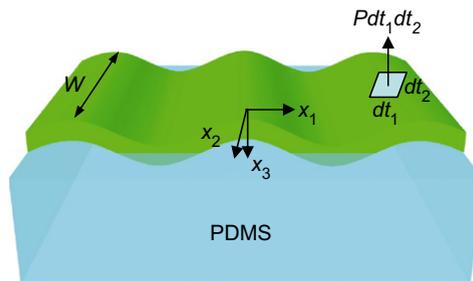
Fig. 4. Schematic illustration of the geometry and coordinate system for a buckled single thin film on PDMS substrate. W is the width of the thin film.

The strain energy in the PDMS substrate is then obtained from Eqs. (14) and (15) as

$$U_s = \frac{k}{4\pi} \int_{x_2=-W/2}^{W/2} \int_{x_1=0}^{\frac{2\pi}{k}} \int_{t_2=-W/2}^{W/2} \beta \cos(kx_1) \frac{2\beta \cos(kx_1)}{\pi \bar{E}_s} Y_0(k|t_2-x_2|) \, dt_2 \, dx_1 \, dx_2$$
$$= \frac{\beta^2 \rho(Wk)}{k^2 \pi \bar{E}_s},$$
(16)

where

$$\rho(x) = -1 + xY_1(x) + x^2 Y_0(x) + \frac{\pi}{2} x^2 [H_1(x)Y_0(x) + H_0(x)Y_1(x)]$$
(17)

is a non-dimensional function, and H_n ($n = 0, 1, 2, \ldots$) denotes the Struve function (Abramowitz and Stegun, 1972).

3.3. Potential energy

The total potential energy Π_{tot} of the system is the sum of membrane and bending energy in the thin film and the strain energy in the substrate. However, for the thin film displacement in Eq. (8) and substrate displacement in Eq. (15) that are continuous only on the average sense, the potential energy becomes

$$\Pi_{tot} = U_b + U_m + U_s - \int \Lambda(w - w_s) dS,$$
(18)

where Λ is the Lagrange multiplier, and the integration is over the film/substrate interface (per unit length). The variation of the above potential energy with respect to Λ would yield $w = w_s$, and the variation with respect to the displacements w and w_s gives Λ to be the traction T_3 (Eq. (11)) at the thin film/substrate interface, and is replaced by T_3 in the following. The potential energy then becomes

$$\Pi_{tot} = -\frac{1}{48} Wh^3 E_f k^4 A^2 + \frac{1}{2} Wh E_f \left(\varepsilon_{pre} - \frac{1}{4} A^2 k^2 \right) \left(\varepsilon_{pre} + \frac{3}{4} A^2 k^2 \right) - \frac{\beta^2 \rho(Wk)}{\pi \bar{E}_s k^2},$$
(19)

which depends on buckling amplitude A and wavelength $\lambda = 2\pi/k$, as well as the film width W.

4. Width effect on buckling wavelength

The minimization of potential energy Π_{tot} in Eq. (19) with respect to the buckling amplitude A, $\partial \Pi_{tot}/\partial A = 0$, gives

$$A = \begin{cases} \frac{2}{k} \sqrt{\varepsilon_{pre} - F}, & F < \varepsilon_{pre}, \\ 0, & F \geqslant \varepsilon_{pre}, \end{cases}$$
(20)

where

$$F = \frac{\pi W \bar{E}_s}{4h E_f \rho(Wk)} + \frac{1}{12} h^2 k^2.$$
(21)

Eq. (20) suggests that the buckling occurs only when the pre-strain reaches a critical value given by Eq. (21), in which the wave number k is to be determined in the following.

The minimization of potential energy with respect to the wave number, $\partial \Pi_{tot}/\partial k = 0$, gives the following nonlinear equation for k:

$$\frac{\bar{E}_s W^3}{E_f h^3} = \frac{4[\rho(Wk)]^2}{3\pi R(Wk)},$$
(22)

where

$$R = 2Y_0(x) + \pi H_1(x) Y_0(x) + \pi H_0(x) Y_1(x)$$
(23)

is a non-dimensional function. The wave number k determined from Eq. (22) has the following dependence on the thin film and substrate elastic properties and film thickness h and width W:

$$k = \frac{1}{h} \left(\frac{3\bar{E}_s}{E_f} \right)^{1/3} f\left[\left(\frac{\bar{E}_s}{E_f} \right)^{1/3} \frac{W}{h} \right],$$
(24)

where f is a non-dimensional function of its variable $(\bar{E}_s/E_f)^{1/3}(W/h)$ to be determined numerically from Eq. (22). The wavelength is $\lambda = 2\pi/k$. Fig. 5 shows the non-dimensional function f versus its variable $(\bar{E}_s/E_f)^{1/3}(W/h)$. It is a universal relation for all film and substrate elastic properties, as well as film width and thickness. As shown in Fig. 5, this universal relation is very well approximated by the simple relation $f(x) \approx \coth[(16/15)(x^{1/4})]$, where coth is the hyperbolic cotangent
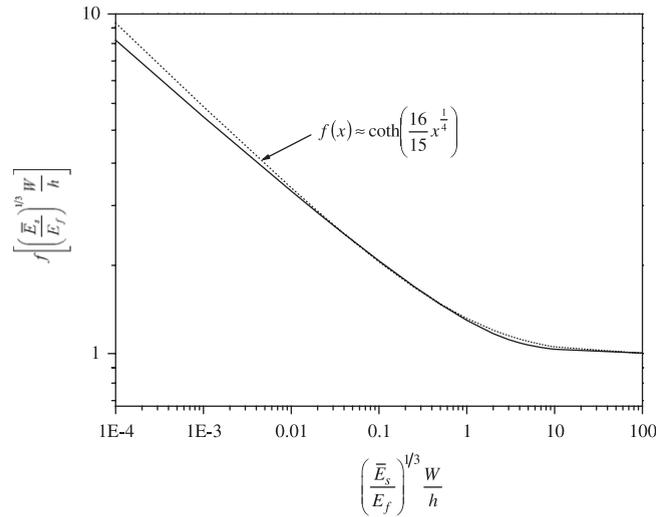
Fig. 5. Plot of dimensionless function $f[(\bar{E}_s/E_f)^{1/3}(W/h)]$ versus a combination parameter $(\bar{E}_s/E_f)^{1/3}(W/h)$. An approximated expression $f(x) \approx \coth[(16/15)(x^{1/4})]$ is given in the dotted line.

function (cosh/sinh). Therefore, the wavelength can be obtained as

$$\lambda = 2\pi h \left(\frac{E_f}{3\bar{E}_s}\right)^{1/3} \tanh\left\{\frac{16}{15}\left[\left(\frac{\bar{E}_s}{E_f}\right)^{1/3}\frac{W}{h}\right]^{1/4}\right\}. \tag{25}$$

Eq. (25) suggests that the dependence of the wave number (or wavelength) on the film width W is always through the non-dimensional parameter $(\bar{E}_s/E_f)^{1/3}(W/h)$. For the limit of very wide film, i.e., $W \to \infty$, $\rho(Wk) = 1/2\pi Wk$ and $R(Wk) = \pi/Wk$ such that f approaches 1, and the wavelength degenerates to that in Eq. (1).

Figs. 6(a and b) show, respectively, the buckling wavelength and amplitude versus the film width for the analytical model in this section (red line) as well as for the experimental results (filled circles) given in Section 2. For experiments in Section 2, the thickness of Si thin film is 100 nm and the pre-strain is 1.3%. The Young's moduli and the Poisson's ratios of Si thin film and PDMS substrate are $E_f = 130$ GPa, $E_s = 2.2$ MPa, $v_f = 0.27$ and $v_s = 0.5$ (INSPEC, 1988; Wilder et al., 2006). It is clear that the buckling profile depends strongly on film width. For example, the buckling wavelength varies from 15.5 μm for 100-μm-wide film to 12.5 μm for 2-μm-wide film. The analytical model in this section agrees very well with experiments.[2]

5. Thin films interactions: film spacing effects

Multiple thin films widely separated on the substrate buckle independently. As the film spacing decreases, mechanical interactions mediated by the underlying substrate become significant. We study the effect of film spacing in this section via the model of two thin films with the same thickness h and width W shown schematically in Fig. 7. The film spacing is s. For large film spacing, the films buckle independently, and the wavelengths and amplitudes are still given by Eqs. (20) and (22). For small film spacing, the two thin films have strong interactions and therefore buckle together with the same wavelength (or wave number k) and same phase.

Following the same approach in Section 3, the distributed force on the top surface of the substrate underneath the film has the same expression as that for single strip in Section 3, and is given by

$$P = -\left[\frac{h^3 E_f}{12}Ak^4 + hE_f\left(\frac{1}{4}A^2k^2 - \varepsilon_{\text{pre}}\right)Ak^2\right]\cos(kx_1) = \beta\,\cos(kx_1), \tag{26}$$

where β is given in Eq. (12).

a

b
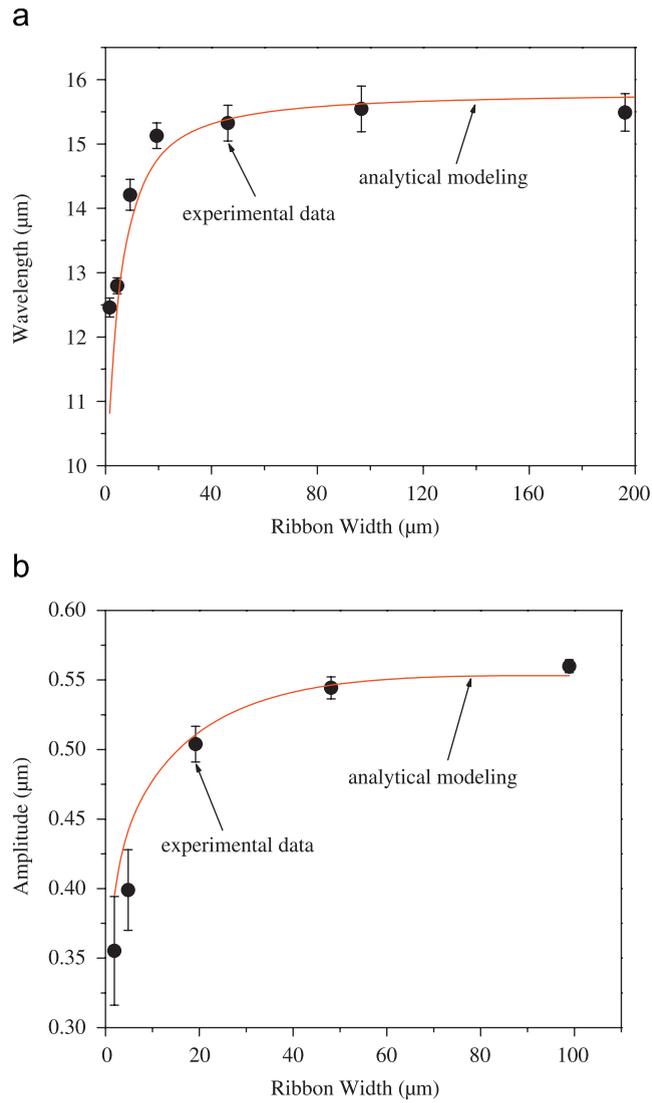
Fig. 6. The buckling profile, wavelength for (a) and amplitude for (b), as a function of the width of silicon thin films. The theoretical analysis is shown in red line and the experimental data are shown in filled circles.
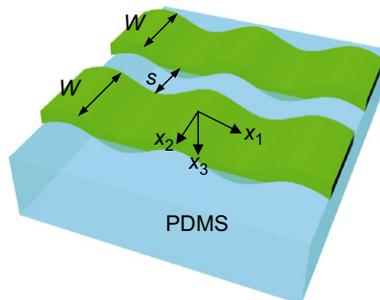
Fig. 7. Schematic illustration of the geometry and coordinate system for two buckled thin films on PDMS substrate, with identical thickness and width W. s is the spacing between two thin films.

Based on the Boussinesq's solution, the normal displacement at the top surface is given by

$$
w_s(x_1, x_2, 0) = \int_{t_2=-W/2}^{W/2} \int_{t_1=-\infty}^{\infty} \frac{\beta \cos(kt_1)}{\pi \bar{E}_s} \frac{1}{\sqrt{(x_1 - t_1)^2 + (x_2 - t_2)^2}} dt_1 dt_2
$$

$$
+ \int_{t_2=W/2+s}^{3W/2+s} \int_{t_1=-\infty}^{\infty} \frac{\beta \cos(kt_1)}{\pi \bar{E}_s} \frac{1}{\sqrt{(x_1 - t_1)^2 + (x_2 - t_2)^2}} dt_1 dt_2, \tag{27}
$$

which can be expressed as

$$
w_s(x_1, x_2, 0) = \frac{2\beta \cos(kx_1)}{\pi \bar{E}_s} \left[\int_{-W/2}^{W/2} Y_0(k|t_2 - x_2|) \, dt_2 + \int_{W/2+s}^{3W/2+s} Y_0(k|t_2 - x_2|) \, dt_2 \right]
$$

$$
= \frac{2\beta \cos(kx_1)}{\pi \bar{E}_s} \left[\int_{-W/2}^{W/2} [Y_0(k|t_2 - x_2|) + Y_0(k|t_2 + W + s - x_2|)] \, dt_2 \right]. \tag{28}
$$

The total potential for substrate and thin films is then obtained as

$$
\Pi_{tot} = WhE_f \left(\varepsilon_{pre} - \frac{1}{4}A^2 k^2 \right) \left(\varepsilon_{pre} + \frac{3}{4}A^2 k^2 \right) - \frac{1}{24}Wh^3 E_f k^4 A^2
$$

$$
- \frac{\beta^2}{\pi \bar{E}_s k^2} \{ 2\rho(Wk) + \rho(sk) - 2\rho[(W+s)k] + \rho[(2W+s)k] \}, \tag{29}
$$

a

b
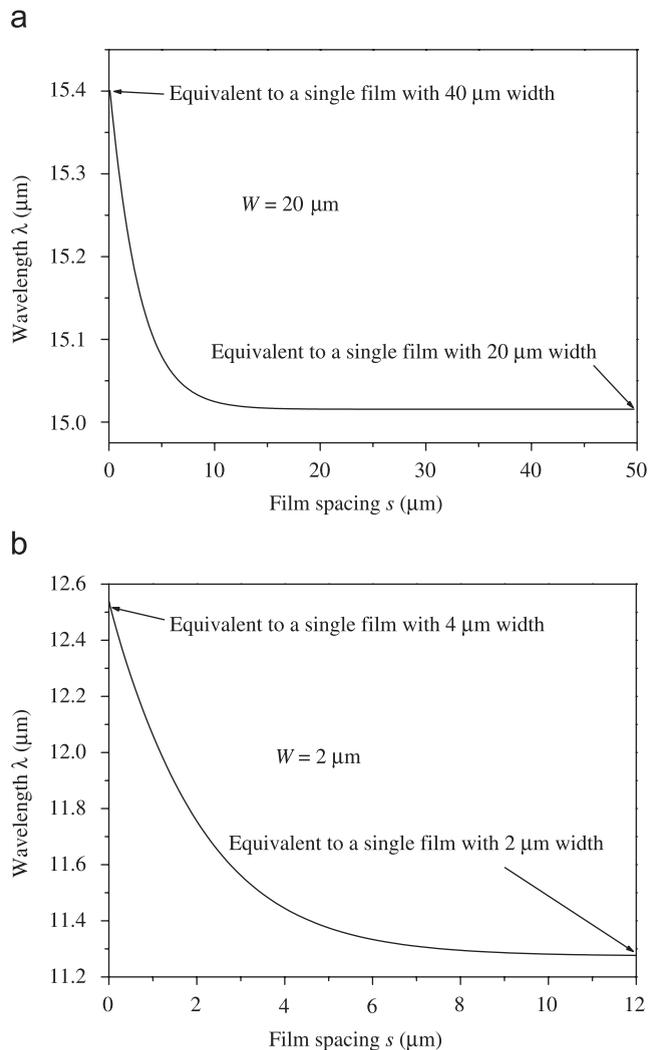
Fig. 8. The buckling wavelength as a function of spacing s between two thin films with identical widths of 20 μm (a) and 2 μm (b).

where the function ρ is given in Eq. (17). Energy minimization gives the wave number and amplitude. Specifically, the wave number k is determined by the following nonlinear equation

$$\frac{1}{3\pi} + \frac{\bar{E}_s W}{kE_f h^3} \frac{d}{dk} \left\{ \frac{1}{2\rho(Wk) + \rho(sk) - 2\rho[(W+s)k] + \rho[(2W+s)k]} \right\} = 0. \tag{30}$$

Fig. 8 shows the wavelength λ versus the film spacing s for two moderately wide thin films (width $W = 20\,\mu m$) and two narrow thin films (width $W = 2\,\mu m$). The material properties and film thickness ($h = 100\,nm$) are the same as those in Fig. 6. For the two limits of film spacing s approaching infinity and zero, the wavelength λ becomes that for a single film of width W and $2W$, respectively. For moderately wide thin films ($W = 20\,\mu m$), the effect of film spacing is almost negligible since the wavelength varies from 15.4 ($s \to \infty$) to 15.0 μm ($s \to 0$). For narrow thin films ($W = 2\,\mu m$), the effect of film spacing is significant, 12.5 ($s \to \infty$)–11.2 μm ($s \to 0$). Only when the film spacing reaches about 3 times the width (i.e., 6 μm) the effect of film spacing disappears.

6. Periodic thin films

Many experiments involve periodic thin films (e.g., Fig. 2), which are studied in this section. Let W denote the thin film width and s the spacing. The normal stress traction on the top surface of PDMS (underneath the thin films) is still given by
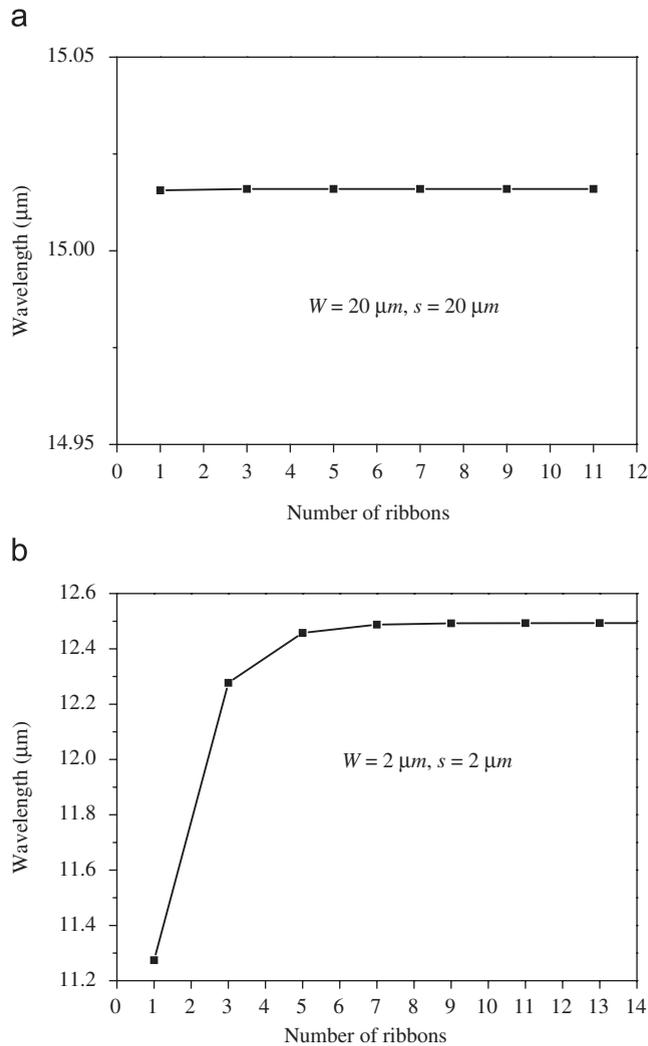
Fig. 9. The buckling wavelength as a function of number of periodic ribbons for (a) 20-μm-wide ribbons periodically separated by 20 μm, and (b) 2-μm-wide ribbons periodically separated by 2 μm.

$P = \beta \cos(kx_1)$ in Eq. (13). The normal displacement on the top surface of the substrate becomes

$$w_s(x_1, x_2, 0) = \frac{4\beta \cos(kx_1)}{\pi \bar{E}_s} \int_{t_2=-W/2}^{W/2} \left\{ \frac{1}{2} Y_0(k|t_2 - x_2|) + \sum_{n=1}^{\infty} Y_0[k|t_2 + n(W+s) - x_2|] \right\} dt_2. \tag{31}$$

The total potential per thin film is given by

$$\Pi_{\text{tot}} = \frac{1}{2} W h E_f \left(\varepsilon_{\text{pre}} - \frac{1}{4} A^2 k^2 \right) \left(\varepsilon_{\text{pre}} + \frac{3}{4} A^2 k^2 \right) - \frac{1}{48} W h^3 E_f k^4 A^2 - \frac{\beta^2}{\pi \bar{E}_s}$$
$$\times \left\langle \rho(Wk) + \sum_{n=1}^{\infty} \{ \rho[n(W+s)k - Wk] - 2\rho[n(W+s)k] + \rho[n(W+s)k + Wk] \} \right\rangle, \tag{32}$$

where the function ρ is given in Eq. (17). The wavelength and amplitude are determined by energy minimization.

Fig. 9 shows the wavelength λ versus number of periodic ribbons for moderately wide thin films (width $W = 20\,\mu m$) and narrow thin films (width $W = 2\,\mu m$). The material properties and film thickness are the same as those in Fig. 6.

a

b
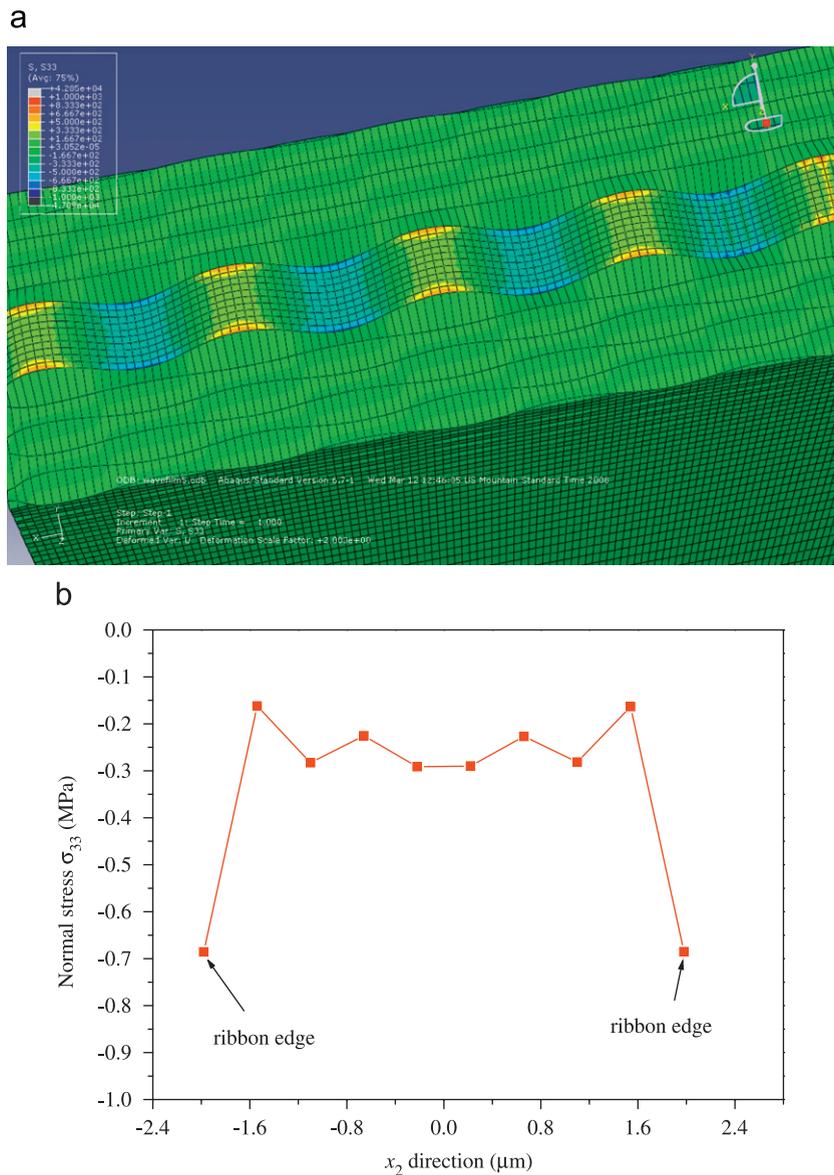
Fig. 10. The normal stress on PDMS top surface obtained by ABAQUS. (a) Contour plot of normal stress and (b) PDMS top surface normal stress along the width direction at one buckling peak.

For moderately wide thin films ($W = 20\,\mu$m), the effect of periodic ribbons is almost neglectable since the wavelength also does not depend on number of ribbons (Fig. 9a). For narrow thin films ($W = 2\,\mu$m), the periodic ribbons are significant because the wavelength seems to saturate up to 9 ribbons.

7. Concluding remarks

Systematic experimental and analytical studies of finite-width stiff thin-films buckling on compliant substrate are presented in this paper. The experimental and analytical results show that both the buckling amplitude and wavelength increase with the film width, and the analytical solution agrees very well with experiments.

This study is important to the fundamental understanding of the buckling behavior of stiff thin films on compliant substrate. It has a wide range of applications, ranging from stretchable electronics (e.g., Khang et al., 2006), precision metrology (Stafford et al., 2004) to sensors and prosthetic devices (Efimenko et al., 2005).

Acknowledgment

Appendix

The normal traction at the film/substrate interface is assumed to be uniform in the x_2 direction in Section 3.2. Such an assumption holds for wide films (width $\gg$ buckle wavelength). For relatively narrow films, we used the finite element analysis (FEA) software ABAQUS to determine the normal stress distribution. A 4.4-μm-wide and 100-nm-thick Si thin film covers the center of the surface of a 100 μm-thick PDMS substrate system, which is subjected to 1.3% compressive strain in thin film direction. The thin film and substrate have the same length 63.5 μm, and are modeled by the plate and three-dimensional brick elements, respectively. To bypass solving the buckling problem using FEA, we introduce a small imperfection that is described by $A \cos[(2\pi/\lambda)(x_1)]$, where $A = 0.05\,\mu$m and $\lambda = 12.7\,\mu$m (based on the analytical analysis given by Eq. (24)). In other words, the thin film has very small initial waveness.

The contour plot of normal stress σ_{33} on PDMS top surface in Fig. 10(a) clearly shows that the normal stress is approximately uniform along the thin film width direction. Fig. 10(b) shows the distribution of normal stress σ_{33} at one buckling peak along the x_2-direction, which confirms the approximate uniformity. This analysis justifies the uniformity of normal stress across the thin film width.

References

Abramowitz, M., Stegun, I.A., 1972. Handbook of Mathematical Functions with Formulas, Graphs, and Mathematical Tables. Dover, New York.
Bowden, N., Brittain, S., Evans, A.G., Hutchinson, J.W., Whitesides, G.M., 1998. Spontaneous formation of ordered structures in thin films of metals supported on an elastomeric polymer. Nature 393 (6681), 146–149.
Bowden, N., Huck, W.T.S., Paul, K.E., Whitesides, G.M., 1999. The controlled formation of ordered, sinusoidal structures by plasma oxidation of an elastomeric polymer. Appl. Phys. Lett. 75 (17), 2557–2559.
Chen, X., Hutchinson, J.W., 2004. Herringbone buckling patterns of compressed thin films on compliant substrates. J. Appl. Mech. Trans. ASME 71 (5), 597–603.
Choi, K.M., Rogers, J.A., 2003. A photocurable poly(dimethylsiloxane) chemistry designed for soft lithographic molding and printing in the nanometer regime. J. Am. Chem. Soc. 125 (14), 4060–4061.
Choi, M.K., Song, J., Khang, D.-K., Jiang, H., Huang, Y., Rogers, J.A., 2007. Biaxially stretchable "Wavy" silicon nanomembranes. Nano Lett. 7 (6), 1655–1663.
Efimenko, K., Rackaitis, M., Manias, E., Vaziri, A., Mahadevan, L., Genzer, J., 2005. Nested self-similar wrinkling patterns in skins. Nat. Mater. 4 (4), 293–297.
Espinosa, H.D., Prorok, B.C., Peng, B., Kim, K.H., Moldovan, N., Auciello, O., Carlisle, J.A., Gruen, D.M., Mancini, D.C., 2003. Mechanical properties of ultrananocrystalline diamond thin films relevant to MEMS/NEMS devices. Exp. Mech. 43 (3), 256–268.
Fu, Y.Q., Sanjabi, S., Barber, Z.H., Clyne, T.W., Huang, W.M., Cai, M., Luo, J.K., Flewitt, A.J., Milne, W.I., 2006. Evolution of surface morphology in TiNiCu shape memory thin films. Appl. Phys. Lett. 89 (17), 3.
Harris, A.K., Wild, P., Stopak, D., 1980. Silicone—rubber substrata-new wrinkle in the study of cell locomotion. Science 208 (4440), 177–179.
Harrison, C., Stafford, C.M., Zhang, W.H., Karim, A., 2004. Sinusoidal phase grating created by a tunably buckled surface. Appl. Phys. Lett. 85 (18), 4016–4018.
Huang, R., 2005. Kinetic wrinkling of an elastic film on a viscoelastic substrate. J. Mech. Phys. Solids 53 (1), 63–89.
Huang, R., Im, S.H., 2006. Dynamics of wrinkle growth and coarsening in stressed thin films. Phys. Rev. E 74 (2), 12.
Huang, R., Suo, Z., 2002a. Instability of a compressed elastic film on a viscous layer. Int. J. Solids Struct. 39 (7), 1791–1802.
Huang, R., Suo, Z., 2002b. Wrinkling of a compressed elastic film on a viscous layer. J. Appl. Phys. 91 (3), 1135–1142.
Huang, R., Yin, H., Liang, J., Sturm, J.C., Hobart, K.D., Suo, Z., 2002. Mechanics of relaxing SiGe islands on a viscous glass. Acta Mech. Sin. 18 (5), 441–456.
Huang, Z.Y., Hong, W., Suo, Z., 2004. Evolution of wrinkles in hard films on soft substrates. Phys. Rev. E 70 (3), 4.
Huang, Z.Y., Hong, W., Suo, Z., 2005. Nonlinear analyses of wrinkles in a film bonded to a compliant substrate. J. Mech. Phys. Solids 53 (9), 2101–2118.
Huck, W.T.S., Bowden, N., Onck, P., Pardoen, T., Hutchinson, J.W., Whitesides, G.M., 2000. Ordering of spontaneously formed buckles on planar surfaces. Langmuir 16 (7), 3497–3501.
INSPEC, 1988. Properties of Silicon. Institution of Electrical Engineers, New York.

Jiang, H., Khang, D.-Y., Song, J., Sun, Y.G., Huang, Y., Rogers, J.A., 2007a. Finite deformation mechanics in buckled thin films on compliant supports. Proc. Nat. Acad. Sci. USA 104, 15607–15612.

Jiang, H., Sun, Y., Rogers, J.A., Huang, Y.Y., 2007b. Mechanics of precisely controlled thin film buckling on elastomeric substrate. Appl. Phys. Lett. 90, 133119.

Jiang, X.Y., Takayama, S., Qian, X.P., Ostuni, E., Wu, H.K., Bowden, N., LeDuc, P., Ingber, D.E., Whitesides, G.M., 2002. Controlling mammalian cell spreading and cytoskeletal arrangement with conveniently fabricated continuous wavy features on poly(dimethylsiloxane). Langmuir 18 (8), 3273–3280.

Kachanov, M., Shafiro, B., Tsukrov, I., 2003. Handbook of Elasticity Solutions. Kluwer Academic Publishers, Boston.

Khang, D.Y., Jiang, H.Q., Huang, Y., Rogers, J.A., 2006. A stretchable form of single-crystal silicon for high-performance electronics on rubber substrates. Science 311 (5758), 208–212.

Kim, T.-H., Choi, W.M., Kim, D.H., Meitl, M.A., Menard, E., Jiang, H., Carlisle, J.A., Rogers, J.A., 2008. Printable, flexible and stretchable forms of ultrananocrystalline diamond with applications in thermal management. Adv. Mater. (in press).

Lacour, S.P., Jones, J., Suo, Z., Wagner, S., 2004. Design and performance of thin metal film interconnects for skin-like electronic circuits. IEEE Electron Device Lett. 25 (4), 179–181.

Lacour, S.P., Jones, J., Wagner, S., Li, T., Suo, Z.G., 2005. Stretchable interconnects for elastic electronic surfaces. Proc. IEEE 93 (8), 1459–1467.

Lacour, S.P., Wagner, S., Huang, Z.Y., Suo, Z., 2003. Stretchable gold conductors on elastomeric substrates. Appl. Phys. Lett. 82 (15), 2404–2406.

Lacour, S.P., Wagner, S., Narayan, R.J., Li, T., Suo, Z.G., 2006. Stiff subcircuit islands of diamond like carbon for stretchable electronics. J. Appl. Phys. 100 (1), 6.

Schmid, H., Wolf, H., Allenspach, R., Riel, H., Karg, S., Michel, B., Delamarche, E., 2003. Preparation of metallic films on elastomeric stamps and their application for contact processing and contact printing. Adv. Funct. Mater. 13 (2), 145–153.

Sharp, J.S., Jones, R.A.L., 2002. Micro-buckling as a route towards surface patterning. Adv. Mater. 14 (11), 799–802.

Stafford, C.M., Guo, S., Harrison, C., Chiang, M.Y.M., 2005. Combinatorial and high-throughput measurements of the modulus of thin polymer films. Rev. Sci. Instrum. 76 (6), 5.

Stafford, C.M., Harrison, C., Beers, K.L., Karim, A., Amis, E.J., Vanlandingham, M.R., Kim, H.C., Volksen, W., Miller, R.D., Simonyi, E.E., 2004. A buckling-based metrology for measuring the elastic moduli of polymeric thin films. Nat. Mater. 3 (8), 545–550.

Stafford, C.M., Vogt, B.D., Harrison, C., Julthongpiput, D., Huang, R., 2006. Elastic moduli of ultrathin amorphous polymer films. Macromolecules 39 (15), 5095–5099.

Sun, Y., Choi, W.M., Jiang, H., Huang, Y.Y., Rogers, J.A., 2006. Controlled buckling of semiconductor nanoribbons for stretchable electronics. Nat. Nanotechnol. 1, 201–207.

Tarasovs, S., Andersons, J., 2008. Buckling of a coating strip of finite width bonded to elastic half-space. Int. J. Solids Struct. 45 (2), 593–600.

Teixeira, A.I., Abrams, G.A., Bertics, P.J., Murphy, C.J., Nealey, P.F., 2003. Epithelial contact guidance on well-defined micro- and nanostructured substrates. J. Cell Sci. 116 (10), 1881–1892.

Timoshenko, S., Gere, J., 1961. Theory of Elastic Stability. McGraw-Hill, New York.

Wagner, S., Lacour, S.P., Jones, J., Hsu, P.H.I., Sturm, J.C., Li, T., Suo, Z.G., 2004. Electronic skin: architecture and components. Phys. E-Low-Dimens. Syst. Nanostruct. 25 (2-3), 326–334.

Wilder, E.A., Guo, S., Lin-Gibson, S., Fasolka, M.J., Stafford, C.M., 2006. Measuring the modulus of soft polymer networks via a buckling-based metrology. Macromolecules 39 (12), 4138–4143.

Yoo, P.J., Suh, K.Y., Park, S.Y., Lee, H.H., 2002. Physical self-assembly of microstructures by anisotropic buckling. Adv. Mater. 14 (19), 1383–1387.